

Analytical model of tilted driver-pickup coils for eddy current nondestructive evaluation

Bing-Hua Cao(曹丙花), Chao Li(李超), Meng-Bao Fan(范孟豹), Bo Ye(叶波), Gui-Yun Tian(田贵云)
Citation: Chin. Phys. B . 2018, 27(3): 030301. **doi:** 10.1088/1674-1056/27/3/030301

Journal homepage: http://cpb.iphy.ac.cn; http://iopscience.iop.org/cpb

What follows is a list of articles you may be interested in

Physical interpretation of Planck's constant based on the Maxwell theory

Donald C Chang(张东才)
Chin. Phys. B . 2017, 26(4): 040301. **doi:** 10.1088/1674-1056/26/4/040301

Inverse problem of pulsed eddy current field of ferromagnetic plates

Chen Xing-Le, Lei Yin-Zhao
Chin. Phys. B . 2015, 24(3): 030301. **doi:** 10.1088/1674-1056/24/3/030301

Characteristics of spectral-hole burning in Tm^{3+}：YAG based on the perturbation theory

Zhang Shi-Yu, Ma Xiu-Rong, Zhang Shuang-Gen, Chen-Lei, Wang Xia-Yang, Mu Kuan-Lin, Wang Song
Chin. Phys. B . 2014, 23(6): 060304. **doi:** 10.1088/1674-1056/23/6/060304

Prediction and experimental measurement of electromagnetic thrust generated by a microwave thruster system

Yang Juan, Wang Yu-Quan, Ma Yan-Jie, Li Peng-Fei, Yang Le, Wang Yang, He Guo-Qiang
Chin. Phys. B . 2013, 22(5): 050301. **doi:** 10.1088/1674-1056/22/5/050301

Research on synthetic aperture radar imaging technology of one-dimensional layered rough surfaces

Ji Wei-Jie, Tong Chuang-Ming
Chin. Phys. B . 2013, 22(2): 020301. **doi:** 10.1088/1674-1056/22/2/020301

Analytical model of tilted driver–pickup coils for eddy current nondestructive evaluation*

Bing-Hua Cao(曹丙花)[1,2], Chao Li(李超)[1,†], Meng-Bao Fan(范孟豹)[2,3], Bo Ye(叶波)[4], and Gui-Yun Tian(田贵云)[5]

[1] School of Information and Control Engineering, China University of Mining and Technology, Xuzhou 221116, China
[2] Jiangsu Key Laboratory of Mine Mechanical and Electrical Equipment, China University of Mining and Technology, Xuzhou 221116, China
[3] School of Mechatronic Engineering, China University of Mining and Technology, Xuzhou 221116, China
[4] Faculty of Information Engineering and Automation, Kunming University of Science and Technology, Kunming 650500, China
[5] School of Electrical and Electronic Engineering, Newcastle University, Newcastle upon Tyne NE1 7RU, UK

(Received 8 August 2017; revised manuscript received 11 December 2017; published online 13 February 2018)

A driver-pickup probe possesses better sensitivity and flexibility due to individual optimization of a coil. It is frequently observed in an eddy current (EC) array probe. In this work, a tilted non-coaxial driver-pickup probe above a multilayered conducting plate is analytically modeled with spatial transformation for eddy current nondestructive evaluation. Basically, the core of the formulation is to obtain the projection of magnetic vector potential (MVP) from the driver coil onto the vector along the tilted pickup coil, which is divided into two key steps. The first step is to make a projection of MVP along the pickup coil onto a horizontal plane, and the second one is to build the relationship between the projected MVP and the MVP along the driver coil. Afterwards, an analytical model for the case of a layered plate is established with the reflection and transmission theory of electromagnetic fields. The calculated values from the resulting model indicate good agreement with those from the finite element model (FEM) and experiments, which validates the developed analytical model.

Keywords: nondestructive evaluation, eddy currents, tilted coils, analytical model

PACS: 03.50.–z, 03.50.De, 41.20.–q, 41.20.Gz **DOI:** 10.1088/1674-1056/27/3/030301

1. Introduction

Eddy current testing (ECT) is extensively used in industries to gauge thickness and conductivity or identify defects for nondestructive evaluation of a part.[1,2] In the simplest case, an ECT probe basically is a coil that receives a magnetic field and generates an alternating excitation field. Nowadays, a driver-pickup probe, consisting of two coils that respectively act as the transmitter and the receiver, has received increasing attention. Such examples can be frequently observed in eddy current array probes.[3,4] Driver-pickup probes have an advantage over one-coil probes in that they have higher gain, wider frequency range, and immunity to thermal drift, because the driver and pickup coil can be individually designed for a specific application.[5] However, a probe sometimes tilts due to surface deformation[3] or poor surface treatment.[6] Basically, eddy current signals are fairly sensitive to probe inclination. The unwanted signal change due to probe tilt is reported to be one of the major obstacles for effective ECT.[6,7] To reduce it, there is a strong demand for powerful, accurate, efficient, and cost-effective tools to investigate the physics.

An analytical model is preferred, because it could establish a mathematical relationship between the signals and the tilt angle of a probe. The signals of a driver-pickup probe are basically the mutual impedance between the driver and pickup coil. Up to date, analytical models of coaxial coils above a layered conductor have been well developed since Dodd and Deeds published their pioneering research results in the late 1960s and the early 1970s.[8] For non-coaxial coils, there are two methods available to deal with the modelling, to the authors' knowledge. One is to use the Lorentz reciprocity relations,[5,9,10] and the other is to integrate over a receiver according to the definition of mutual impedance, which is easier to implement.[11–13] However, for a tilted driver-pickup probe, the latter method is confronted with difficulties in integrating over the pickup coil. Therefore, the analytical modelling of a tilted driver-pickup probe with the second method is still an open problem.

The main contribution of this paper lies in that spatial transformation is employed to derive the mapped vector of the MVP from the driver coil onto the vector along the tilted pickup coil, thus developing an analytical model of a coaxial driver-pickup probe above a layered planar conductor. The remainder of this paper is organized as follows. In Section 2, we formulate the closed-form expressions for two misaligned filamentary loops in the translational and tilted mode respectively. Subsequently, an analytical model of mutual impedance change from a tilted driver-pickup probe is developed following the methods of Dodd and Deeds and the pro-

*Project supported by the National Natural Science Foundation of China (Grant Nos. 61701500, 51677187, and 51465024).
†Corresponding author. E-mail: finchlee@cumt.edu.cn
© 2018 Chinese Physical Society and IOP Publishing Ltd

cedures for numerical implementation are described in Section 3. Then, the established model is validated by FEM and in experiment in Section 4, and a discussion is carried out in Section 5. Finally, some conclusions are drawn from this work in Section 6.

2. Analytical expressions for non-coaxial filamentary loops

In the following analysis, a driver is assumed to carry a sinusoidal signal with the frequency ω, and phasor notation is employed.[10]

2.1. Formulation for translational loops

We consider two circular filaments as shown in Fig. 1. The driver loop is located at the origin $O(0,0,0)$ of the plane xOy, and its axis coincides with the axis z. The distances between the driver and pickup loop are L in the vertical direction and D in the horizontal direction, respectively. The (r_d,ϕ,z) is the coordinate of a field point, and r_p is the radius of the pickup loop.

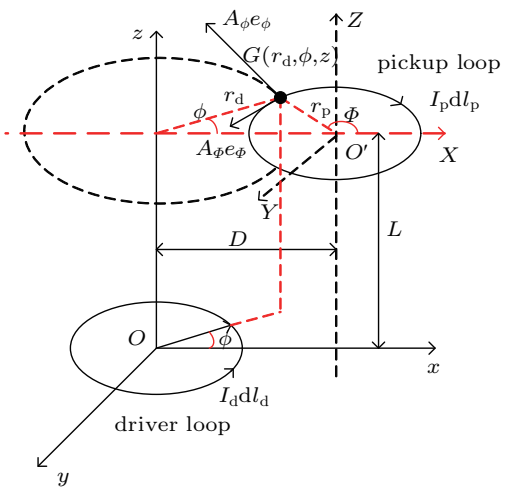


Fig. 1. (color online) Misaligned filamentary loops.

The formulation of MVP for the driver loop has been developed.[14] In the cylindrical coordinate system, there is only the circumferential component $A_\phi(r_\mathrm{d},z)$ when considering the axial symmetry of MVP. The $A_\Phi(r_\mathrm{p},z)$ is the scalar projection of $A_\phi(r_\mathrm{d},z)e_\phi$ on e_Φ. According to Faraday's law, the mutual impedance between the two circular filaments is

$$\begin{aligned} Z_{12} &= \frac{\mathrm{j}\omega}{I_\mathrm{d}}\oint_{l_\mathrm{p}} A_\Phi(r_\mathrm{p},z)e_\Phi\cdot\mathrm{d}l_\mathrm{p} = \frac{\mathrm{j}\omega}{I_\mathrm{d}}\int_0^{2\pi} A_\Phi(r_\mathrm{p},z)r_\mathrm{p}\mathrm{d}\Phi \\ &= \frac{\mathrm{j}\omega}{I_\mathrm{d}}\int_0^{2\pi} A_\phi(r_\mathrm{d},z)e_\phi\cdot e_\Phi r_\mathrm{p}\mathrm{d}\Phi, \end{aligned} \tag{1}$$

where I_d is the amplitude of the current flowing into the driver loop.

From Eq. (1), we can see that building the relationship between $A_\Phi(r_\mathrm{p},z)$ and $A_\phi(r_\mathrm{d},z)$ plays a key role. From Fig. 2 it follows that $A_\Phi(r_\mathrm{p},z)$ is

$$A_\Phi(r_\mathrm{p},z) = A_\phi(r_\mathrm{d},z)\cos\alpha, \tag{2}$$

where α is the angle between $A_\phi(r_\mathrm{d},z)e_\phi$ and e_Φ.

According to the triangle exterior angle theorem, α is

$$\alpha = \Phi - \phi. \tag{3}$$

On the basis of the law of cosines, r_d is derived as

$$r_\mathrm{d} = \sqrt{D^2 + r_\mathrm{p}^2 + 2Dr_\mathrm{p}\cos\Phi}. \tag{4}$$

The angle ϕ could be described as

$$\begin{aligned} \phi &= \arccos\frac{D + r_\mathrm{p}\cos\Phi}{r_\mathrm{d}} \\ &= \arccos\frac{D + r_\mathrm{p}\cos\Phi}{\sqrt{D^2 + r_\mathrm{p}^2 + 2Dr_\mathrm{p}\cos\Phi}}, \quad \phi\in[0,\pi]. \end{aligned} \tag{5}$$

Substituting Eqs. (2)–(5) into Eq. (1) yields

$$Z_{12} = \frac{\mathrm{j}\omega}{I_\mathrm{d}}\int_0^{2\pi}\cos\alpha A_\phi(r_\mathrm{d},L)r_\mathrm{p}\mathrm{d}\Phi. \tag{6}$$

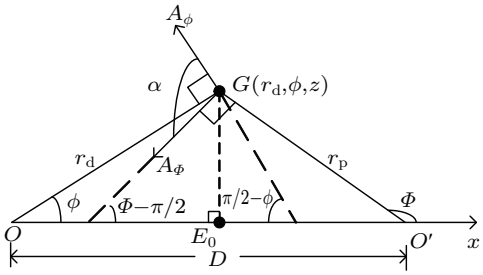


Fig. 2. Relations between the angles Φ and ϕ.

2.2. Formulation for tilted loops

The geometry of the tilted loops in free space is shown in Fig. 3, where the center of the pickup loop is placed at the point O', and φ is the angle between the unit normal vector of the pickup loop and the z-axis direction.

According to Eq. (1), finding the relation between the vector $A_\phi(r_\mathrm{d},z)$ and $A_\Phi(r_\mathrm{p},z)$ is also critical for tilted filamentary loops. The process is divided into two steps. Firstly, the MVP from the tilted pickup loop is mapped onto a horizontal plane as illustrated in Fig. 4. Then, we use the method in Subsection 2.1 to build the relation between $A_\phi(r_\mathrm{d},z)$ and $A_\Phi(r_\mathrm{p},z)$.

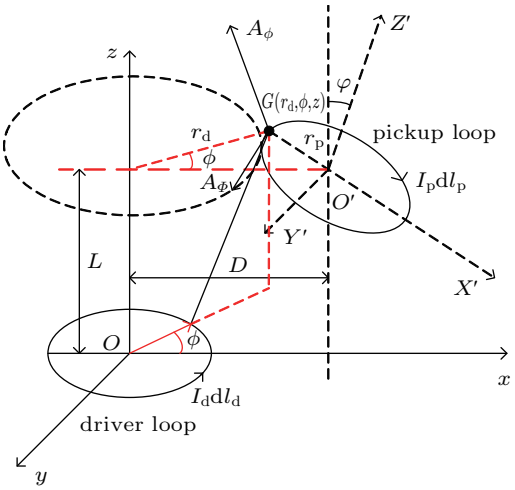


Fig. 3. (color online) Tilted filamentary loops.

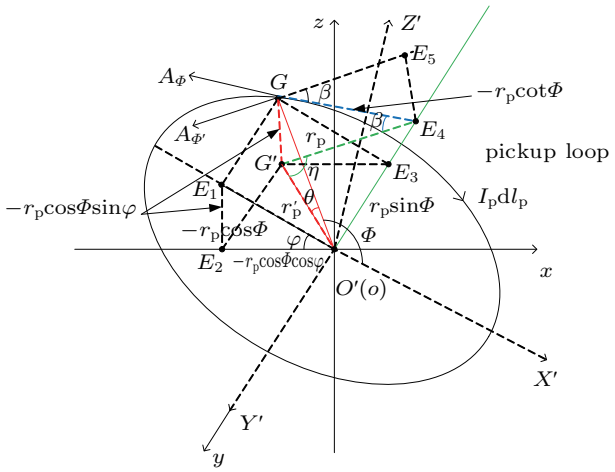


Fig. 4. (color online) Mapped pickup loop onto a horizontal plane.

The projection of $A_\Phi(r_p,z)\boldsymbol{e}_\Phi$ onto a horizontal plane is given by

$$A_{\Phi'} = A_\Phi \cos\beta, \tag{7}$$

where β is the angle between $A_\Phi \boldsymbol{e}_\Phi$ and its projected vector $A_{\Phi'}\boldsymbol{e}_{\Phi'}$.

From Figs. 5 and 6, the angle β could be expressed as

$$\beta = \arcsin\frac{GG'}{GE_4} = \arcsin(\sin\Phi\sin\varphi), \quad \beta \in \left(0, \frac{\pi}{2}\right). \tag{8}$$

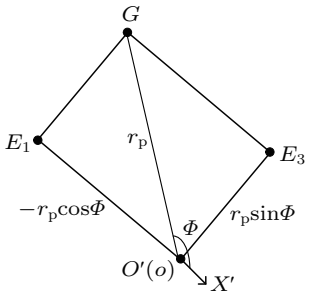


Fig. 5. Diagram of r_p.

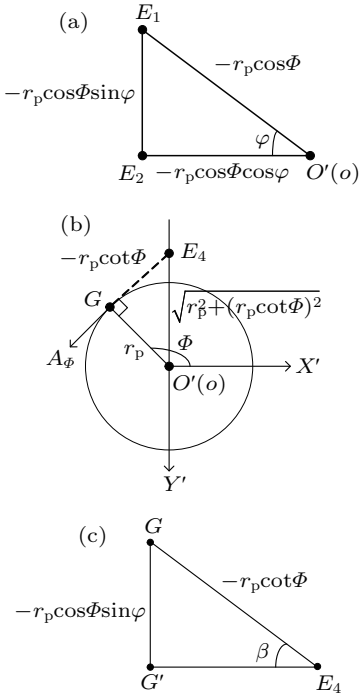


Fig. 6. Characterization of the angle β. (a) The angle φ. (b) The angle Φ. (c) The angle β.

Figure 7 shows that $r'_p \boldsymbol{e}_{\Phi'}$ is the mapped vector of $r_p \boldsymbol{e}_\Phi$ onto a horizontal plane. Then, r'_p and Φ' are given by

$$r'_p = \sqrt{(r_p\cos\Phi\cos\varphi)^2 + (r_p\sin\Phi)^2}, \tag{9}$$

$$\Phi' = \arccos\frac{r_p\cos\Phi\cos\varphi}{r'_p}, \quad \Phi' \in [0,\pi]. \tag{10}$$

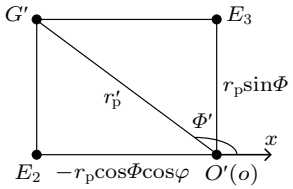


Fig. 7. The angle Φ' and r'_p.

The θ is the angle between the vector $O'G'$ and the vector $O'G$ as shown in Fig. 8. It is obvious that θ is

$$\theta = \arcsin\frac{GG'}{oG} = -\arcsin(\cos\Phi\sin\varphi), \quad \theta \in \left(-\frac{\pi}{2}, \frac{\pi}{2}\right). \tag{11}$$

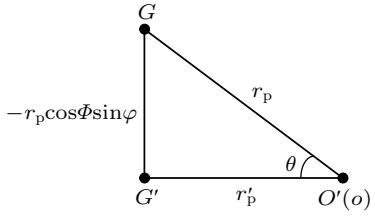


Fig. 8. The angle θ.

The η is the angle between $A_{\Phi'}\boldsymbol{e}_{\Phi'}$ and $O'G'$ as shown in Fig. 9. According to the law of cosines, η is

$$\eta = \arccos \frac{(r_{\rm p}\cos\theta)^2 + (r_{\rm p}\cot\Phi\cos\beta)^2 - [r_{\rm p}^2 + (r_{\rm p}\cot\Phi)^2]}{2r_{\rm p}\cos\theta r_{\rm p}\cot\Phi\cos\beta}. \tag{12}$$

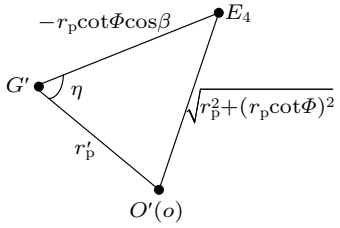


Fig. 9. The angle η.

The scalar projection $A_{\Phi'}$ of $A_\phi(r_{\rm d},z)\boldsymbol{e}_\phi$ on $\boldsymbol{e}_{\Phi'}$ gives

$$A_{\Phi'} = A_\phi\cos\alpha', \tag{13}$$

where α' is the angle between $A_\phi(r_{\rm d},z)\boldsymbol{e}_\phi$ and $\boldsymbol{e}_{\Phi'}$ as shown in Fig. 10.

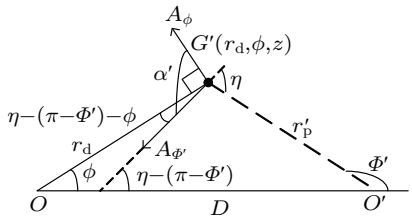


Fig. 10. Relations between the angles Φ' and ϕ.

We follow the method in Subsection 2.1 to build the relationship between $A_{\Phi'}$ and A_Φ. Further, combining Eq. (7) with Eq. (13), the mathematical relationship between $A_\Phi(r_{\rm p},z)$ and $A_\phi(r_{\rm d},z)$ is

$$A_\Phi(r_{\rm p},z) = \frac{\cos\alpha'}{\cos\beta}A_\phi(r_{\rm d},z), \tag{14}$$

where

$$\alpha' = \Phi' + \eta - \phi - \frac{\pi}{2}, \quad r_{\rm d} = \sqrt{D^2 + (r'_{\rm p})^2 + 2Dr'_{\rm p}\cos\Phi'}.$$

Using Eq. (14), equation (1) for the case of the tilted loops becomes

$$Z_{12} = \frac{{\rm j}\omega}{I_{\rm d}}\int_0^{2\pi}\frac{\cos\alpha'}{\cos\beta}A_\phi(r_{\rm d},L)r_{\rm p}{\rm d}\Phi. \tag{15}$$

3. Analytical modeling for driver-pickup coils above layered plates

For the eddy current nondestructive evaluation, a coil is of typically multilayer and multi-turn as shown in Fig. 11. The driver and pickup coils are separated by the distance D in the horizontal direction and the distance L in the vertical direction. The driver coil consists of $N_{\rm d}$ turns and has inner radius $r_{1{\rm d}}$, outer radius $r_{2{\rm d}}$, and the thickness $2h_{\rm d}$. The pickup coil has $N_{\rm p}$ turns and has inner radius $r_{1{\rm p}}$, outer radius $r_{2{\rm p}}$, and the thickness $2h_{\rm p}$. The pickup coil axis lies on the plane $y = D$ and is tilted by an angle φ with respect to the surface normal. The q-th $(q = 1,2,3,\ldots,k-1)$ layer has a conductivity of σ_q, a magnetic permeability of μ_q, and a thickness of $c_{q+1} - c_q$.

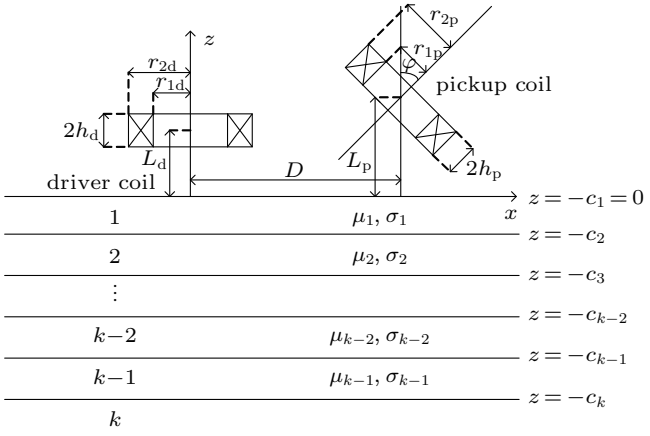


Fig. 11. Tilted coils above a layered plate.

The total magnetic field above the conductor could be considered as the superposition of the excitation $A^{(\rm s)}$ and EC field $A^{(\rm ec)}$

$$A = A^{(\rm s)} + A^{(\rm ec)}. \tag{16}$$

The EC field $A^{(\rm ec)}$ could be regarded as the reflection of $A^{(\rm s)}$.[14–16] By imposing an artificial magnetic insulation boundary at the radial distance $r_{\rm d} = h$,[17,18] $A^{(\rm ec)}$ is represented in a series-form expression as

$$A^{(\rm ec)}(r_{\rm d},z) = \sum_{i=1}^{\infty} K_i C_{{\rm II},i} R'_{0i,1i}(\lambda_{0i}){\rm e}^{-\lambda_{0i}z}, \tag{17}$$

where

$$K_i = n_{\rm cd}\mu_0 I_{\rm d} J_1(\lambda_{0i}r_{\rm d})\frac{\chi(\lambda_{0i}r_{1{\rm d}},\lambda_{0i}r_{2{\rm d}})}{\lambda_{0i}^4}\frac{1}{[hJ_0(\lambda_{0i}h)]^2},$$
$$C_{{\rm II},i} = {\rm e}^{-\lambda_{0i}(L_{\rm d}-h_{\rm d})} - {\rm e}^{-\lambda_{0i}(L_{\rm d}+h_{\rm d})},$$
$$n_{\rm cd} = \frac{N_{\rm d}}{2h_{\rm d}(r_{2{\rm d}}-r_{1{\rm d}})},$$

J_n denotes the n-order Bessel function, μ_0 is the permeability of free space,

$$J_1(\lambda_{0i}h) = 0, \tag{18}$$

λ_{0i} is the i-th positive root,

$$\chi(x_1,x_2) = \int_{x_1}^{x_2} xJ_1(x){\rm d}x, \tag{19}$$

$R'_{0i,1i}(\lambda_{0i})$ is the generalized reflection coefficient which is defined as the ratio of $A^{(\mathrm{ec})}$ to $A^{(\mathrm{s})}$, and could be easily formulated with the reflection and transmission theory of electromagnetic field[14–16] or Cheng's Matrix method.[19] It is described as[14]

$$R'_{qi,(q+1)i} = \frac{R_{qi,(q+1)i} + R'_{(q+1)i,(q+2)i} \mathrm{e}^{-2\lambda_{(q+1)i}(c_{q+1}-c_q)}}{1 + R_{qi,(q+1)i} R'_{(q+1)i,(q+2)i} \mathrm{e}^{-2\lambda_{(q+1)i}(c_{q+1}-c_q)}}, \quad (20)$$

where

$$R_{qi,(q+1)i} = \frac{\mu_{q+1}\lambda_{qi} - \mu_q \lambda_{(q+1)i}}{\mu_{q+1}\lambda_{qi} + \mu_q \lambda_{(q+1)i}},$$
$$R'_{(k-1)i,ki} = R_{(k-1)i,ki},$$
$$\lambda_{qi} = \sqrt{\lambda_{0i}^2 + \mathrm{j}\omega\sigma_q\mu_q}.$$

Using the approach of Dodd and Deeds, the discrete nature of the windings is neglected, and the change in mutual impedance can be deduced from Eq. (15) by taking the cylindrical coil as a countless ideal combination of single-turn coils. Therefore, the mutual impedance change between the driver and pickup coils is

$$\Delta Z_{12} = \frac{\mathrm{j}\omega n_{\mathrm{cp}}}{I_{\mathrm{d}}} \int_{L_{\mathrm{p}}-h_{\mathrm{p}}}^{L_{\mathrm{p}}+h_{\mathrm{p}}} \int_{r_{1\mathrm{p}}}^{r_{2\mathrm{p}}} \int_0^{2\pi} r_{\mathrm{p}} \frac{\cos\alpha'}{\cos\beta} A^{(\mathrm{ec})} \times (r_{\mathrm{d}}, z)\mathrm{d}\Phi\mathrm{d}r_{\mathrm{p}}\mathrm{d}z. \quad (21)$$

Substituting Eq. (17) into Eq. (21) and performing the integration, the resulting equation is as follows:

$$\Delta Z_{12} = \mathrm{j}\omega\mu_0 n_{\mathrm{cd}} n_{\mathrm{cp}} \int_{r_{1\mathrm{p}}}^{r_{2\mathrm{p}}} \int_0^{2\pi} B \sum_{i=1}^{\infty} D_i \times \frac{(\mathrm{e}^{-\lambda_{0i}(L_{\mathrm{p}}-h_{\mathrm{p}})} - \mathrm{e}^{-\lambda_{0i}(L_{\mathrm{p}}+h_{\mathrm{p}})})(\mathrm{e}^{-\lambda_{0i}(L_{\mathrm{d}}-h_{\mathrm{d}})} - \mathrm{e}^{-\lambda_{0i}(L_{\mathrm{d}}+h_{\mathrm{d}})})}{\lambda_{0i}} \times R'_{0i,1i}(\lambda_{0i})\mathrm{d}\Phi\mathrm{d}r_{\mathrm{p}}, \quad (22)$$

where

$$n_{\mathrm{cp}} = \frac{N_{\mathrm{p}}}{2h_{\mathrm{p}}(r_{2\mathrm{p}} - r_{1\mathrm{p}})},$$
$$B = r_{\mathrm{p}} \frac{\cos\alpha'}{\cos\beta},$$
$$D_i = J_1(\lambda_{0i} r_{\mathrm{d}}) \frac{\chi(\lambda_{0i} r_{1\mathrm{d}}, \lambda_{0i} r_{2\mathrm{d}})}{\lambda_{0i}^4} \frac{1}{[hJ_0(\lambda_{0i} h)]^2}.$$

Generally, it is required that the numerical integration should predict the change of mutual impedance. Now we adopt the Gauss–Legendre algorithm to compute the integral in Eq. (22). The procedures are as follows.

Step 1: Divide equally the intervals $[r_{1\mathrm{p}}, r_{2\mathrm{p}}]$ and $[0, 2\pi]$ into ten subintervals, respectively.

Step 2: For each subinterval of $[r_{1\mathrm{p}}, r_{2\mathrm{p}}]$, perform numerical integration over each subinterval of $[0, 2\pi]$.

Step 3: Sum the integration results over the subintervals of $[0, 2\pi]$.

Step 4: Repeat steps 2 and 3 until the integration over the subintervals of $[r_{1\mathrm{p}}, r_{2\mathrm{p}}]$ is completed.

4. FEM simulation and experiment

4.1. FEM simulation

Finite element model (FEM) is a popular and powerful tool to investigate EC phenomena.[20–22] In this paper, a three-dimensional (3D) FEM for layered structures was developed by using ANSYS Maxwell to implement the simulations. It is noted that the computational burden and accuracy of an FEM are mesh-dependent. Considering the balance between efficiency and accuracy, the maximum length of the elements in the coils was set to be 0.5 mm. For the layered sample, the number of the meshed layers was set to be 5, and the maximum length of the surface triangle elements was set to be 4 mm. The meshed elements would increase by 30% after each iteration. The maximum number of iterations was set to be 20 in order to derive the converged solution of the developed FEM.

4.2. Experiment

The theoretical results presented in Section 3 were validated experimentally. The fabricated coils were almost identical in dimension as listed in Table 1. Using a caliper, the inner radius of a coil was measured beforehand. After the fabrication of the coils, the outer radii and height were gauged. The self-inductance and resonant frequency of the isolated coils were recorded from the readings of a Wayne Kerr WK65120B impedance analyzer, and the DC resistance was measured using a digital multimeter.[23] The parameters of the manufactured samples are shown in Table 2. The conductivities of the prepared samples were provided by Xiamen Tianyan Instruments Ltd which is an electrical conductivity meter manufacturer. The prepared samples were large enough in dimensions compared with the coils to remove edge effects.[14]

Table 1. Coil parameters.

	Driver coil	Pickup coil
inner radius/mm	$r_{1\mathrm{d}} = 8.00$	$r_{1\mathrm{p}} = 8.00$
outer radius/mm	$r_{2\mathrm{d}} = 10.00$	$r_{2\mathrm{p}} = 10.00$
thickness/mm	$2h_{\mathrm{d}} = 17.00$	$2h_{\mathrm{p}} = 17.00$
number of turns	$N_{\mathrm{d}} = 136$	$N_{\mathrm{p}} = 134$
coil center height/mm	$L_{\mathrm{d}} = 18$	$L_{\mathrm{p}} = 18$
coil center distance/mm	$D = 36$	$D = 36$
isolated coil inductance/Mh	$L_{0\mathrm{d}} = 0.21$	$L_{0\mathrm{p}} = 0.21$
DC resistance/Ω	$R_{0\mathrm{d}} = 1.00$	$R_{0\mathrm{p}} = 1.00$
free-space resonant frequency/MHz	$f_{\mathrm{Rd}} = 6.32$	$f_{\mathrm{Rp}} = 6.54$

Table 2. Sample parameters.

	Plate P1 (Al 3003)
Thickness/mm	$c = 3.00$
electrical conductivity/MS·m^{-1}	$\sigma = 35.00$
relative magnetic permeability	$\mu_{\mathrm{r}} = 1.00$
lateral dimensions/mm^2	100×100

The schematic experimental setup for ECT is shown in Fig. 12. The mutual impedance was measured using an SR830 DSP lock-in amplifier working in the gain-phase mode. From Fig. 13, it is found that the amplitude and phase of mutual impedance could be calculated with the ratio v of $V_{\rm TEST}$ to $V_{\rm REF}$, where $V_{\rm TEST}$ denotes the secondary voltage in a pickup coil and $V_{\rm REF}$ is the voltage of the resistor $R_{\rm REF}$.[10] A PC recorded experimental results from the lock-in amplifier via GPIB communication using a customized software developed in LabVIEW. The coil was rotated by a rotatable platform, and the targeted tilt angle was obtained through a protractor.

In experiment, a two-layer case was investigated to validate the developed analytical model. In the case an aluminum plate (P1) and air layer are combined; the frequency of the signal fed into the driver coil increases from 10 Hz to 100 kHz.

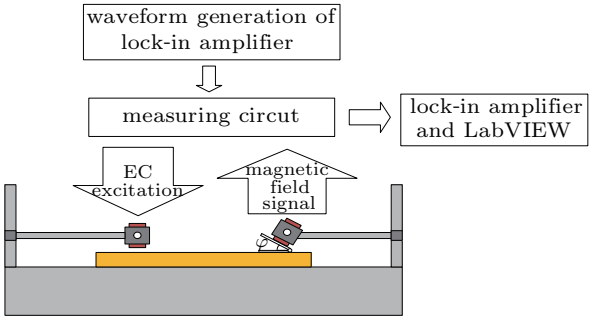


Fig. 12. (color online) Schematic of ECT experimental setup.

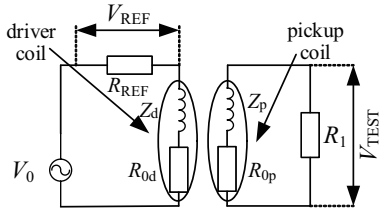


Fig. 13. Circuit for measurement of mutual impedance.

Figure 13 illustrates the circuit for measuring the mutual impedance, and Table 3 displays the parameters in the circuit.

Table 3. Circuit parameters.

	Circuit
driving voltage	V_0
driver coil impedance	$Z_{\rm d}$
driver coil DC resistance/Ω	$R_{0\rm d} = 1.00$
standard resistor/Ω	$R_{\rm REF} = 22$
voltage across a standard resistor	$V_{\rm REF}$
pickup coil impedance	$Z_{\rm p}$
pickup coil DC resistance/Ω	$R_{0\rm p} = 1.00$
input resistance/MΩ	$R_1 = 1$
voltage across the pickup coil	$V_{\rm TEST}$

The change in mutual inductance is defined as

$$\Delta M = \Delta Z_{12}/(\mathrm{j}\omega). \tag{23}$$

Equation (23) indicates that the change in mutual inductance is a frequency-dependent complex number. From Fig. 13, the ratio v of the voltage $V_{\rm TEST}$ to $V_{\rm REF}$ is

$$v = \frac{V_{\rm TEST}}{V_{\rm REF}} = \frac{\mathrm{j}\omega M}{R_{\rm REF}} \frac{1}{1 + (R_{0\rm p} + Z_{\rm p})/R_1}. \tag{24}$$

When the input resistance R_1 is on the order of a megaohm, the real and imaginary parts of mutual inductance are given in terms of the magnitude $|v|$ and phase θ by[10]

$$\begin{aligned} \mathrm{Re}\, M &= \frac{R_{\rm REF}\,|v|}{\omega} \sin\theta, \\ \mathrm{Im}\, M &= -\frac{R_{\rm REF}\,|v|}{\omega} \cos\theta. \end{aligned} \tag{25}$$

5. Results and discussion

In experiment, the driver coil is arranged to be parallel to the sample. Then, the changes in mutual impedances are observed and recorded when the driver coil is titled by angles of 0°, 45°, 60°, and 90° in sequence. Subsequently, simulations are carried out with the formulated analytical model and developed FEM. The experimental and calculated results are shown in Fig. 14.

On the whole, the results from the formulated analytical model match well with those from the FEM and experiments. The differences fall within 5%. The good agreement indicates the validation of the presented analytical model. Further analysis suggests that the observed deviations in a low frequency range are less than those in a high frequency range. It is also found that the imaginary parts are superior to the real parts in accuracy.

In the formulated analytical model and FEM, a coil is assumed to be a pure inductor. However, it is reported that an experimental coil has parasitic stray capacitance.[24] Therefore, a disparity basically exists between the calculations and measurements. In addition, the measurement errors also result from coil parameters and tilt angle.

The model is independent of the mesh and offers series-form expression.[25] It presents an efficient and accurate tool to calculate mutual impedance due to a specimen. The developed analytical model can be beneficial to physics-based signal explanation[26] and inverse process to characterize the defects.[10]

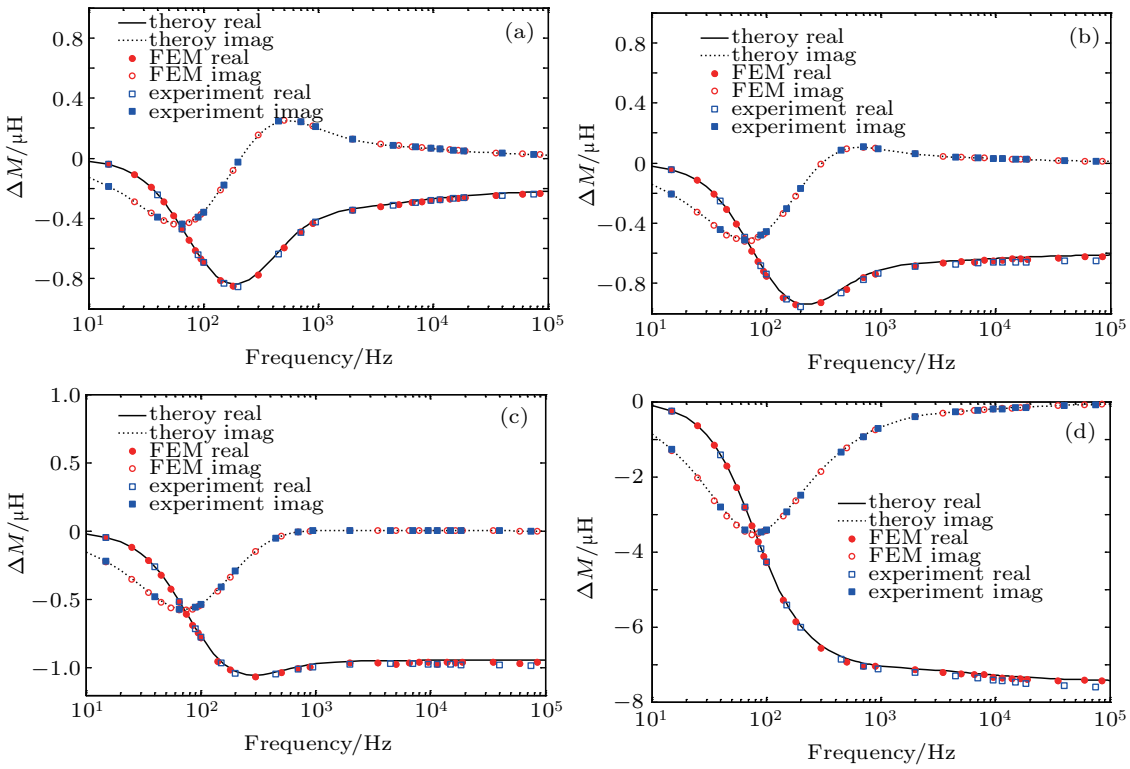


Fig. 14. (color online) Variations of mutual inductance with frequency for (a) $\varphi = 0°$, (b) 45°, (c) 60°, and (d) 90°.

6. Conclusions

In this paper, an analytical model for the change in mutual impedance of a non-coaxial driver-pickup probe due to multi-layered conductors is established by using spatial transformation, TREE method and reflection and transmission theory of electromagnetic fields. Instead of utilizing the Lorentz reciprocity relations, this work formulates the induced voltage by integrating over a pickup coil. Such an approach is easy to follow, and the resulting analytical model is simple for numerical implementation.

The presented model enables us to have an in-depth insight into the signal variations due to probe tilt, thus facilitating to find a feature immune to probe tilt. In addition, the developed model could also be used to compute the incident field to improve the efficiency of a forward solver from the volume integral method.

Acknowledgment

The authors would like to thank the Xiamen Tianyan Instruments Ltd for measuring the conductivities of the samples free of charge.

References

[1] Sophian, Tian G Y, Fan M B, *et al.*2017 *Mech. Eng.* **30** 500
[2] Rosell A 2015 *NDT&E Int.* **75** 48
[3] Chao X, Li Y and Nie J 2016 *J. Magn.* **21** 524
[4] Sun Z, Cai D, Zou C, *et al.* 2017 *Meas. Sci. Technol.* **28** 045105
[5] Theodoulidis T P and Ditchburn R J 2007 *IEEE Trans. Magn.* **43** 3368
[6] Yang G, Zeng Z, Deng Y, *et al*. 2012 *NDT&E Int.* **52** 1
[7] Li Y, Sheng X, Lian M, *et al*. 2015 *NDT&E* **31** 289
[8] Dodd C V and Deeds W E 1968 *J. Appl. Phys.* **39** 2829
[9] Ge D B and Wei B 2012 *Acta Phys. Sin.* **61** 050301 (in Chinese)
[10] Burke S K and Ibrahim M E 2004 *J. Phys. D: Appl. Phys.* **37** 1857
[11] Burke S K and Ditchburn R J 2008 *Res. Nondestr. Eval.* **19** 1
[12] Li Y, Chen Z and Qi Y 2011 *IEEE Trans. Magn.* **47** 2931
[13] Yin W, Binns R, Dickinson S J, *et al.* 2007 *IEEE Trans. Instrum. Meas.* **56** 2775
[14] Fan M B, Huang P J, Ye B, *et al.* 2009 *Acta Phys. Sin.* **58** 5950 (in Chinese)
[15] Fan M B, Cao B H and Yang X F 2010 *Acta Phys. Sin.* **59** 7570 (in Chinese)
[16] Fan M B, Yin Y D and Cao B H 2012 *Acta Phys. Sin.* **61** 088105 (in Chinese)
[17] Zhang Q and Wu X J 2017 *Acta Phys. Sin.* **66** 038102 (in Chinese)
[18] Theodoulidis T P and Bowler J R 2005 *Proceed. Roy. Soc. Lon. A: Math., Phys. & Eng. Sci.* **461** 3123
[19] Cheng C C 1971 *Int. J. Nondestr. Test.* **3** 109
[20] Huang L, He R and Zeng Z 2012 *IEEE Trans. Magn.* **48** 2161
[21] Li W, Chen G, Yin X, *et al.* 2013 *NDT&E Int.* **53** 31
[22] Miorelli R, Reboud C, Theodoulidis T, *et al.* 2013 *IEEE Trans. Magn.* **49** 2886
[23] Fan M B, Cao B H, Yang P P, *et al.* 2015 *NDT&E Int.* **74** 66
[24] Harrison D J, Jones L D, Burke S K 1996 *J. Nondestr. Eval.* **15** 21
[25] Li Y, Theodoulidis T P and Tian G Y 2007 *IEEE Trans. Magn.* **43** 4010
[26] Fan M B, Cao B H, Sunny A I, *et al.* 2017 *NDT&E Int.* **86** 123